A Multi-Dimensional Virtual Characteristic Scheme for Laminar and Turbulent Incompressible Flows

S. E. Razavi and M. Hanifi [†]

School of Mechanical Engineering, University of Tabriz, Tabriz, East Azerbaijan, 51666-14766, Iran

†*Corresponding Author Email: m_hanifi@tabrizu.ac.ir*

ABSTRACT

A multi-dimensional virtual characteristic-based scheme (MVCB) by the aid of artificial compressibility is developed for convective fluxes in laminar and turbulent incompressible flows. The proper combinations of compatibility equations are determined to obtain primitive variables on cell interfaces. The Reynolds averaged Navier-Stokes equations joined with Spalart-Allmaras turbulent model are solved by finite volumes. This scheme is applied to the flows between parallel plates, over backward-facing step, and in square lid-driven cavity at a wide range of Reynolds numbers. A FORTRAN 90 code has been written and all the results have come out from this code. Several comparisons confirm the scheme ability in accurate simulation of flows without need to any artificial viscosity in laminar and turbulent regimes.

NOMENCLATURE

A	area for 2D cell	U	primitive variables vector
c_{b1} , c_{b2} , c_{t3} , c_{t4} , c_{v1} , c_{w1} , c_{w2} , c_{w3}, σ , κ	constants for Spalart-Allmaras equation	u, v	x, and y components of mean velocity vector
		u_m	Average axial velocity
E, F	flux vectors	$vol.$	cell volume
f	Fanning friction factor	x, y	Cartesian coordinates
f_w , f_{t2} , f_{v1} , f_{v2} , g , r , $\hat{s}$, s , χ , Ω_{ij}	functions for Spalart-Allmaras equation	y_w	distance to the nearest wall in computational domain
H	source term matrix	β	artificial compressibility parameter
l_e	entrance length	Γ	artificial compressibility matrix
P	mean pressure divided by density	ρ	density
p	pressure	ν	kinematic viscosity
Re	Reynolds number	ν_T	turbulent eddy viscosity
t	time	$\hat{\nu}$	modified turbulent viscosity
		$\partial vol.$	lateral face of cell volume

1. INTRODUCTION

Attempts for solving the incompressible Navier-Stokes equations have been made to overcome the defect of velocity-pressure decoupling. Most approaches using primitive variables can be classified into two broad categories, namely the projection and artificial compressibility methods. In the projection methods (either pressure or velocity-correction), at each time step, a sequence of decoupled elliptic equations for the velocity and pressure are solved. The CFRscheme proposed byHarichandan and Roy (2012) is included in this

category. The cell face center velocities are reconstructedexplicitly by solving the momentum equations on fluxreconstruction control volumes defined around the respective cell face centers. This is followedby solution of the cell center pressure field using adiscrete Poisson equation developed from thereconstructed velocities and updating the cell centervelocities by using an explicit scheme.A review of projection methods can be found in Guermond *et al*. (2006).

In artificial compressibility methods, the hyperbolic structure of equations is achieved by adding a pseudo-time derivative of the pressure to the continuity equation (Chorin 1997).

Upwind schemes versus central differencing (or averaging) add inherent artificial viscosity based on the physics of the problem which eliminates the need for any artificial dissipation terms and coefficients. By the aid of artificial compressibility, various kinds of upwind schemes originally designed for compressible flows have been developed to incompressible problems. Rogers and Kwak (1991) developed the flux-difference splitting of Roe in conjunction with the pseudo-compressibility to incompressible Navier-Stokes equations. Upwind scheme is derived from one-dimensional considerations, and applied to each coordinate direction normal and parallel to cell faces separately. Flux-difference splitting was used to bias the differencing based on the sign of eigenvalues of the convective flux Jacobian. Pappou and Tsangaris (1997) developed Steger and Warming's flux vector splitting upwind method by the aim of artificial compressibility for steady laminar incompressible flows. Convective fluxes normal and parallel to control surfaces were decomposed to positive and negative parts in accordance with the sign of the eigenvalues of the Jacobian matrices. From various upwind discretizations, it was reported that MUSCL third-order scheme with Van Albada limiter (to guarantee monotonic behavior in regions with steep pressure gradients) have a better behavior. The scheme being presented by Calhoon and Roach (1997) was utilized interpolating functions for evaluating the control surface fluxes including viscous terms. These functions were derived from direct integration of one-dimensionally linearized forms of momentum equations. Pressure was assumed to be piecewise linear between nodes for integrating procedure. The values achieved from interpolating functions for adjacent cells were different; so the averaged values were applied to gain a conservative procedure. These expressions being dependent to cell Reynolds number, hence, upwind nature of fluxes were obtained. It was claimed without any detail that an artificial compressibility term was applied to time marching procedure. The scheme was applied to lid-driven cavity in the laminar regime.

Above mentioned upwind methods determine only the direction of propagation of information, i.e. upstream or downstream. In characteristic methods the paths of information propagation are determined. The majority of characteristic-based schemes utilize flux splitting in directions perpendicular to cell faces.

Boukir *et al*. (1994) analyzed high order in time splitting characteristics combined with finite element spatial discretization for incompressible Navier-Stokes equations. The characteristic curves were obtained by means of solution to the Cauchy problem with k-th order in time approximated velocity field. Then, weighted values of velocities along characteristics were used to approximate the time derivative for solving the Stokes equation.

Drikakis *et al*. (1994) introduced the characteristic-based (CB) scheme with artificial compressibility for solving laminar flows by Navier-Stokes equations. Locally one-dimensional flow is assumed and compatibility equations were derived from the split Euler equations. The variables on characteristics were computed by an upwind finite difference scheme with third-order interpolation formula based on the sign of local eigenvalues of Jacobian matrix. An upwind-type scheme for cross-derivatives was applied. Flows in the cascade of circular airfoils and over backward-facing step were simulated. Zhao and Zhang (2000) developed Drikakis CB scheme in finite-volume framework, along with energy equation for simulation of laminar incompressible flows on the unstructured grids for a variety of benchmarks. Govatsos and Papantonis (2000) developed the CB scheme for steady turbulent flows. In which, standard k–ε model, together with standard wall functions were applied. The turbulence equations are numerically decoupled from the Navier–Stokes equations. The turbulence equations were discretized by an upwind-type scheme of second-order accuracy according to the velocity direction (Hirsch 1988). The laminar and turbulent flows in square channel with 90-degree bend and in the impeller of a water pump were simulated. Neofytou (2007) revised the CB scheme. To clarify the difference of revised form and original CB, it should be said that Drikakis obtained an algebraic expression with linear combination of split form of governing equations along characteristic paths. Compatibility equations were constructed following the determination of combination coefficients by assuming zero multipliers for spatial derivatives of algebraic expression. Neofytou pointed out that there was a relation between these coefficients that was forgotten in CB scheme and inserting this restriction formed the revised compatibility equations. However, Su *et al*. (2007) analyzed the formulations of the original CB scheme and proved the consistency with the governing flow equations after that convergence has been achieved. Comparisons of original and revised CB schemes were performed by simulation of flow over circular cylinder at Re = 40. The results of both schemes have identical accuracy and convergence rate, despite the fact that original form is simpler.

The characteristic-based split (CBS) finite element scheme was founded byZienkiewicz and Codina (1995) for compressible and incompressible flows. The characteristic Galerkin convection-diffusion process was applied for a scalar quantity to

Table 1 Coefficients for the Spalart- Allmaras model

$c_{b1} = 0.1355$	$c_{b2} = 0.622$	$\sigma = 2/3$	$\kappa = 0.41$	$c_{w1} = 3.2391$
$c_{w2} = 0.3$	$c_{w3} = 2$	$c_{v1} = 7.1$	$c_{t3} = 1.3$	$c_{t4} = 0.5$

discretize the total derivative along the characteristics. This process involves splitting the equation into two parts which one of them contains the convective term and the other one includes diffusion and source terms. It was shown that Navier-Stokes equations in the conservative form could be discretized in time using the characteristic Galerkin method if the variation of pressure is known. Afterwards, semi-implicit and explicit forms of fractional step algorithm were introduced; where intermediate momentum is computed and after determination of pressure and velocity fields the other transport equations, e.g. energy, turbulent quantities, could be computed. Explicit form with artificial compressibility with and without intermediate step was applied to steady incompressible flows over an airfoil and lid-driven cavity (Zienkiewicz *et al*. 1995). Nithiarasu and Liu (2006) applied the CBS scheme to solve turbulent incompressible flows at moderate Reynolds numbers. Boussinesq's hypothesis was applied to Reynolds stresses. Also, Wolfesstain, Spallart-Allmaras, and standard κ-ε models were used for turbulence modeling. The scheme was tested for the channel, backward-facing step, cylinder, and flow in upper human airway.

Razavi *et al*. (2008) proposed an upwind scheme based on multidimensional characteristics (MCB) for laminar incompressible Navier-Stokes equations. Compatibility equations were applied to compute convective fluxes normal to the cells faces. The results of flow in lid-driven cavity were compared with that of CB and averaging schemes. Later, the MCB scheme was developed for body-fitted grids (Zamzamian and Razavi 2008) and examined for flow over backward-facing step and cylinder. The MCB scheme demonstrated very good accuracy and convergence.

Here, virtual wave propagation paths are obtained and used to determine the convective fluxes. The major features include grid independence, keeping the conservative nature of multidimensional characteristics, and throwing away the elaboration by means of omitting spatial derivatives. The scheme is applied and tested on laminar and turbulent flows, which shows very good performance regarding the others.

2. GOVERNING EQUATIONS

Non-dimensional system of Reynolds averaged Navier–Stokes (RANS) equations joined with artificial compressibility, in vector form are expressed as follows,

$$\frac{\partial}{\partial t}\iint_{vol.} \boldsymbol{U} dA + \Gamma \oint_{\partial vol.} (\mathbf{F} dy - \mathbf{E} dx) = \Gamma \iint_{vol.} \boldsymbol{H} dA$$

$$\boldsymbol{U} = \begin{bmatrix} P \\ u \\ v \\ \hat{v} \end{bmatrix}, \qquad \Gamma = \begin{bmatrix} \beta^2 & 0 & 0 & 0 \\ 0 & 1 & 0 & 0 \\ 0 & 0 & 1 & 0 \\ 0 & 0 & 0 & 1 \end{bmatrix}$$

$$\boldsymbol{F} = \begin{bmatrix} u \\ P + u^2 - \left(\frac{1+v_T}{Re}\right)\frac{\partial u}{\partial x} \\ uv - \left(\frac{1+v_T}{Re}\right)\frac{\partial v}{\partial x} \\ u\hat{v} - \left(\frac{1+c_{b2}}{Re\sigma}\right)(1+\hat{v})\frac{\partial \hat{v}}{\partial x} \end{bmatrix}$$

$$\boldsymbol{E} = \begin{bmatrix} v \\ uv - \left(\frac{1+v_T}{Re}\right)\frac{\partial u}{\partial y} \\ P + v^2 - \left(\frac{1+v_T}{Re}\right)\frac{\partial v}{\partial y} \\ v\hat{v} - \left(\frac{1+c_{b2}}{Re\sigma}\right)(1+\hat{v})\frac{\partial \hat{v}}{\partial y} \end{bmatrix}$$

$$\boldsymbol{H} = \left[0,0,0, c_{b1}(1-f_{t2})\hat{s}\hat{v} - \frac{c_{b2}}{Re\sigma}(1+\hat{v})\left(\frac{\partial^2 \hat{v}}{\partial x^2} + \frac{\partial^2 \hat{v}}{\partial y^2}\right) - \frac{1}{Re}\left[c_{w1}f_w - \frac{c_{b1}}{\kappa^2}f_{t2}\right]\left(\frac{\hat{v}}{y_w}\right)^2 \right]^T$$

(1)

where β denotes the artificial compressibility parameter, u and v the mean velocity components, and P the mean pressure divided by density. The laminar shear stress and Reynolds stress tensors are derived by Boussinesq's assumption. v_T shows the turbulent eddy viscosity which is calculated by means of turbulence model. The last row denotes the Spalart-Allmaras equation (SA) having the following specifications; $\hat{v}$, the modified turbulent viscosity which can be expressed as Blazek (2001),

$$v_T = \hat{v} f_{v1}, \quad f_{v1} = \chi^3/(\chi^3 + c_{v1}^3),$$

$$\chi = \hat{v}/v, f_{t2} = c_{t3} exp(-c_{t4}\chi^2),$$

$$\hat{s} = s + \left(\frac{\hat{v}}{\kappa^2 y_w^2}\right) f_{v2}, \quad s = \sqrt{2\Omega_{ij}\Omega_{ij}},$$

$$\Omega_{ij} = \frac{1}{2}\left(\frac{\partial u_i}{\partial x_j} - \frac{\partial u_j}{\partial x_i}\right), \quad f_{v2} = 1 - \frac{\chi}{1+\chi f_{v1}},$$

$$f_w = g\left[\frac{1+c_{w3}^6}{g^6 + c_{w3}^6}\right]^{\frac{1}{6}}, g = r + c_{w2}(r^6 - r),$$

$$r = \frac{\hat{v}}{\hat{s}\kappa^2 y_w^2}$$

(2)

where, v shows the kinematic viscosity, and y_w denotes the distance to the nearest wall in computational domain. The constants of Eqs. (2) are introduced in Table 1.

The scales used for non-dimensional form of RANS and SA model are as follows:

$$u_i^{**} = \frac{\bar{u}_i}{U_{ref}}, x_i^{**} = \frac{\bar{x}_i}{L_{ref}}, p^{**} = \frac{\bar{p}}{\rho_{ref}U_{ref}^2},$$

$$\rho^{**} = \frac{\rho}{\rho_{ref}}, P^{**} = \frac{p^{**}}{\rho^{**}}, t^{**} = \frac{tU_{ref}}{L_{ref}},$$

$$v_T^{**} = \frac{v_T}{v} \; , \hat{v}^{**} = \frac{\hat{v}}{v} \; , Re = \frac{U_{ref} L_{ref}}{v},$$

$$\hat{s} = \frac{U_{ref}}{L_{ref}} \hat{s}^{**}, \hat{s}^{**} = s^{**} + \frac{1}{Re} \left(\frac{\hat{v}^{**}}{\kappa^2 y_w^{**2}} \right) f_{v2},$$

$$s^{**} = \sqrt{2\Omega_{ij}^{**} \Omega_{ij}^{**}}, \Omega_{ij}^{**} = \frac{1}{2} \left(\frac{\partial u_i^{**}}{\partial x_j^{**}} - \frac{\partial u_j^{**}}{\partial x_i^{**}} \right),$$

$$r = \frac{1}{Re} \left(\frac{\hat{v}^{**}}{\hat{s}^{**} \kappa^2 y_w^{**2}} \right)$$

$$(3)$$

Reference values are taken to be the mean inlet values, otherwise described individually in some cases. For facility the "**" has been omitted.

Pressure and velocity components of flux vectors of Eq. (1), F and E, are computed by means of multi-dimensional virtual characteristic-based (MVCB) method that expressed in section 4. Turbulent variables, $\hat{v}$ and v_T, at the cell interfaces are computed by averaging. It is obvious that, for laminar case studies, v_T is set to zero and 4th row of equations is omitted. Viscous terms are calculated on the secondary volumes. This procedure is clarified for a generic term by Eq. (4) and Fig.1.

$$\left(\frac{\partial u}{\partial x} \right)_{bc} = \frac{1}{A_{ObNc}} \iint_{S_{ObNc}} \frac{\partial u}{\partial x} dx dy = \frac{1}{A_{ObNc}} \oint_{ObNcO} u dy$$
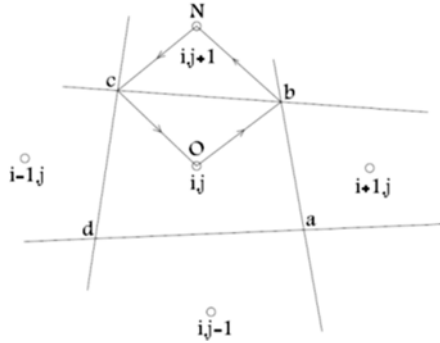
$$(4)$$

Fig. 1. A secondary volume for computing viscous terms.

3. SPATIAL AND TIME DISCRETIZATIONS

On a structured grid, Eq. (1) can be written in discrete form for cell (i,j) as,

$$A_{ij} \frac{\partial U_{ijk}}{\partial t} = -Q_{ijk} k = 1,2,3,4$$

$$Q_{ijk} = \Gamma \left[\sum_{l=1}^{4} \left(F_{ijk} \Delta y - E_{ijk} \Delta x \right)_l \right. $$

$$\left. - A_{ij} F_{ijk} \right]$$

$$(5)$$

where, A indicates the cell area and subscript *k* shows the rows of equations. For expansions of Q_{ijk}, see Appendix A. For computing U_{ijk}, the

following fifth-order Runge-Kutta method is utilized (Blazek 2001),

$$U_{ijk}^{(l)} = U_{ijk}^{(n)} - \alpha_l \frac{\Delta t}{A_{ij}} Q_{ijk}^{(l-1)}$$

$$l = 1,2,...,5 \qquad \alpha_l = \frac{1}{4}, \frac{1}{6}, \frac{3}{8}, \frac{1}{2}, 1 \qquad (6)$$

$$U_{ijk}^{(n+1)} = U_{ijk}^{(5)}$$

4. MVCB SCHEME FOR CONVECTIVE FLUX COMPUTATION

Taking the linear combination of governing equations results in (Zucrow and Hoffman 1977),

$$\omega_1 \left(\frac{\partial P}{\partial t} + \beta^2 \frac{\partial u}{\partial x} + \beta^2 \frac{\partial v}{\partial y} \right)$$

$$+ \omega_2 \left(\frac{\partial u}{\partial t} + u \frac{\partial u}{\partial x} + v \frac{\partial u}{\partial y} \right.$$

$$\left. + \frac{\partial P}{\partial x} \right) \qquad (7)$$

$$+ \omega_3 \left(\frac{\partial v}{\partial t} + u \frac{\partial v}{\partial x} + v \frac{\partial v}{\partial y} \right.$$

$$\left. + \frac{\partial P}{\partial y} \right) = 0$$

By defining the vectors, $\boldsymbol{W_1} = \omega_2 \boldsymbol{i} + \omega_3 \boldsymbol{j} + \omega_1 \boldsymbol{k}$, $\boldsymbol{W_2} = (\beta^2 \omega_1 + u\omega_2)\boldsymbol{i} + v\omega_2 \boldsymbol{j} + \omega_2 \boldsymbol{k}$, and $\boldsymbol{W_3} = u\omega_3 \boldsymbol{i} + (\beta^2 \omega_1 + v\omega_3)\boldsymbol{j} + \omega_3 \boldsymbol{k}$, the following relation can be obtained

$$d_{\boldsymbol{W_1}} P + d_{\boldsymbol{W_2}} u + d_{\boldsymbol{W_3}} v = 0, \qquad d_{\boldsymbol{W_j}} \equiv \boldsymbol{W_j} . \boldsymbol{\nabla} \quad (8)$$

Hence, one can determine the characteristic surface including $\boldsymbol{W_1}$, $\boldsymbol{W_2}$, and $\boldsymbol{W_3}$ with a normal vector ($\boldsymbol{\Psi} = cos\,\theta\,\boldsymbol{i} + sin\,\theta\,\boldsymbol{j} + \eta \boldsymbol{k}$). Performing dot product $\boldsymbol{\Psi} . \boldsymbol{W_j} = 0$, yields

$$\begin{cases} (\eta)\omega_1 + (cos\,\theta)\omega_2 + (sin\,\theta)\omega_3 = 0 \\ (\beta^2 cos\,\theta)\omega_1 + (u\,cos\,\theta + v\,sin\,\theta + \eta)\omega_2 = 0 \quad (9) \\ (\beta^2 sin\,\theta)\omega_1 + (u\,cos\,\theta + v\,sin\,\theta + \eta)\omega_3 = 0 \end{cases}$$

There are two possibilities to have nontrivial solutions for Eq. (9), as

$$u\,cos\,\theta + v\,sin\,\theta + \eta = 0 \qquad (10)$$

$$u\,cos\,\theta + v\,sin\,\theta + \eta = \frac{\beta^2}{\eta} \qquad (11)$$

Combining Eqs. (9) and (10) and plugging into Eq. (7) results in the first compatibility equation

$$sin\,\theta \left(\frac{\partial P}{\partial x} + \frac{\partial u}{\partial t} + u \frac{\partial u}{\partial x} + v \frac{\partial u}{\partial y} \right)$$

$$- cos\,\theta \left(\frac{\partial P}{\partial y} + \frac{\partial v}{\partial t} \right. \qquad (12)$$

$$\left. + u \frac{\partial v}{\partial x} + v \frac{\partial v}{\partial y} \right) = 0$$

The second compatibility equation, corresponding to Eq. (11) is obtained similarly as

$$-\eta \cos\theta \left(\frac{\partial P}{\partial x} + \frac{\partial u}{\partial t} + u\frac{\partial u}{\partial x} + v\frac{\partial u}{\partial y}\right)$$
$$- \eta \sin\theta \left(\frac{\partial P}{\partial y} + \frac{\partial v}{\partial t}\right.$$
$$+ u\frac{\partial v}{\partial x} + v\frac{\partial v}{\partial y}\right) + \frac{\partial P}{\partial t} \qquad (13)$$
$$+ \beta^2 \left(\frac{\partial u}{\partial x} + \frac{\partial v}{\partial y}\right) = 0$$

To derive the expressions for $\frac{d}{dt} = \frac{\partial}{\partial t} + \frac{dx}{dt}\frac{\partial}{\partial x} + \frac{dy}{dt}\frac{\partial}{\partial y}$ along characteristic lines one can assume a characteristic path $f(x, y, t) = 0$ on a characteristic surface. The gradient of f is parallel to the normal vector of this surface and also, perpendicular to the tangent line in each point on it. Therefore, the following relation holds

$$\eta + \frac{dx}{dt}\cos\theta + \frac{dy}{dt}\sin\theta = 0 \qquad (14)$$

Combining Eqs. (10) and (14) results in,

$$D^s = \frac{\partial}{\partial t} + u\frac{\partial}{\partial x} + v\frac{\partial}{\partial y} \qquad (15)$$

where, D^s denotes the substantial derivative along characteristic lines on surfaces corresponds to Eq. (10) and pseudo-pathline (Zucrow and Hoffman 1977). Similarly, substantial derivative corresponding to Eq. (11) can be obtained,

$$D^\theta = \frac{\partial}{\partial t} + \left(u - \frac{\beta^2}{\eta}\cos\theta\right)\frac{\partial}{\partial x} + \left(v - \frac{\beta^2}{\eta}\sin\theta\right)\frac{\partial}{\partial y} \qquad (16)$$

where, D^θ denotes the other kind of substantial derivative varying with θ. Applying Eq. (16), the compatibility Eq. (13) can be written as,

$$-\eta(\theta)\cos\theta\, D^\theta u - \eta(\theta)\sin\theta\, D^\theta v + D^\theta P$$
$$+ \beta^2 \left(\frac{\partial u}{\partial x} + \frac{\partial v}{\partial y}\right.$$
$$- \cos^2\theta\frac{\partial u}{\partial x}$$
$$- \cos\theta\sin\theta\frac{\partial u}{\partial y}$$
$$- \cos\theta\sin\theta\frac{\partial v}{\partial x}$$
$$- \sin^2\theta\frac{\partial v}{\partial y}\right) \qquad (17)$$
$$- \frac{\partial P}{\partial x}\left(u - \frac{\beta^2}{\eta(\theta)}\cos\theta\right.$$
$$+ \eta(\theta)\cos\theta\right)$$
$$- \frac{\partial P}{\partial y}\left(v - \frac{\beta^2}{\eta(\theta)}\sin\theta\right.$$
$$+ \eta(\theta)\sin\theta\right) = 0$$

where, η could be derived from Eq. (11) as a positive function of θ,

$$\eta(\theta)$$
$$= \frac{1}{2}\left(-u\cos\theta - v\sin\theta\right.$$
$$+ \sqrt{(u\cos\theta + v\sin\theta)^2 + 4\beta^2}\right) \qquad (18)$$

Eq. (17) contains local and substantial derivatives

which make it complicated for using in numerical application. In the next step, it is shown that how the simpler relations can be achieved. By selecting compatibility equations for $\theta = 0$, $\frac{\pi}{2}$, π, $\frac{3\pi}{2}$, and pseudo-pathline, the following equations are obtained after algebraic manipulations. For details see Appendix B.

$$-\eta(0)D^0 u - \eta(\pi)D^\pi u + D^\pi P - D^0 P = 0 \qquad (19)$$

$$-\eta(\pi/2)D^{\pi/2}v - \eta(3\pi/2)D^{3\pi/2}v$$
$$+ D^{\pi/2}P - D^{3\pi/2}P = 0 \qquad (20)$$

$$-\eta(0)D^0 u + \eta(\pi)D^\pi u - \eta(\pi/2)D^{\pi/2}v$$
$$+ \eta(3\pi/2)D^{3\pi/2}v$$
$$+ D^0 P + D^{\pi/2}P + D^\pi P \qquad (21)$$
$$+ D^{3\pi/2}P - 2D^s P = 0$$

The most interesting feature of Eqs. (19) to (21) lies in the appearance of non-local derivatives which cause the data propagation on characteristic lines in a straightforward manner.

For evaluating convective fluxes in Eq. (1), the values of variables on cell edge (shown by superscript "*"), are computed from characteristic lines by means of Eqs. (19) to (21). Hence, one gets the following

$$u^* = \frac{1}{\eta(0) + \eta(\pi)}[\eta(0)u^0 + \eta(\pi)u^\pi + P^\pi$$
$$- P^0] \qquad (22)$$

$$v^* = \frac{1}{\eta(\pi/2) + \eta(3\pi/2)}[\eta(\pi/2)v^{\pi/2}$$
$$+ \eta(3\pi/2)v^{3\pi/2}$$
$$+ P^{3\pi/2} - P^{\pi/2}] \qquad (23)$$

$$P^* = \frac{1}{2}[\eta(0)(u^* - u^0) - \eta(\pi)(u^* - u^\pi)$$
$$+ \eta(\pi/2)(v^* - v^{\pi/2})$$
$$- \eta(3\pi/2)(v^* - v^{3\pi/2}) \qquad (24)$$
$$+ P^0 + P^{\pi/2} + P^\pi$$
$$+ P^{3\pi/2} - 2P^s]$$

The intersections of characteristic lines with previous time step are found by means of Eqs. (15) and (16), as

$$x^s = x^* - \Delta t u, \quad y^s = y^* - \Delta t v$$
$$x^\theta = x^* - \Delta t\left(u - \frac{\beta^2}{\eta(\theta)}\cos\theta\right),$$
$$y^\theta = y^* - \Delta t\left(v - \frac{\beta^2}{\eta(\theta)}\sin\theta\right) \qquad (25)$$

Various interpolation methods may be adopted to assign proper data in these intersections. In present work, the first-order interpolation has been used.

5. NUMERICAL RESULTS

The proposed scheme was applied for flow simulations in a channel, over backward-facing step, and for lid-driven cavity in the laminar and turbulent regimes. Boundary conditions in the channel flow were set at the inlet, $u = 1, v = 0, \hat{v} =$

0.1 and P extrapolated from the internal cells. On the side walls, velocity components and $\hat{v}$ were set to zero, and again P was extrapolated from the inside domain. At the outlet, pressure was set to zero, and velocity components along with $\hat{v}$ were extrapolated from internal cells. In the backward-facing step flow, $u, v, and\, \hat{v}$ were extracted from channel flow outlet as inlet boundary condition and P was extrapolated from inside. On the walls and outlet, similar procedures to channel flow were applied. In the cavity, velocity components on sliding wall set as, $u = 1, v = 0,$ and fix walls are treated like channel flow. The parameter β was set to 5 for laminar, and 1 for turbulent flows.

Fig.2 illustrates the geometry of channel and backward-facing step and grids. In the backward-facing step, *L1=6H* for the laminar flows and for turbulent flows, *4H* at *Re = 3025* and *5H* at *Re = 10000, 69610*. Also *L2=60H* for the laminar flows, and for the turbulent equals to *36H* at *Re = 3025* and *25H* at *Re = 10000, 69610*. In the channel flow, *L= L2*.
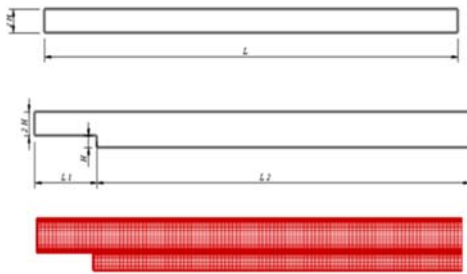
Fig. 2. Geometries of the channel and backward-facing step and grids.

The following convergence criteria was used,

$$ENORM = \frac{\sqrt{\sum_{i=1}^{no.of\,cells}\left(|V|_i^{n+1} - |V|_i^n\right)^2}}{\sqrt{\sum_{i=1}^{no.of\,cells}\left(|V|_i^{n+1}\right)^2}} \quad (26)$$

To insure grid independence, the simulations for various cell numbers were conducted for different cases. Fig.3 shows the u-velocity profile in the fully developed region of turbulent channel flow at *Re=3025* for cell numbers, 2500, 4096, and 6400.

Fig.4 compares the convergence histories of the turbulent flow over backward-facing step for MVCB and averaging schemes at *Re*=3025, 10000, 69610, and 500000. Superiority of the MVCB scheme without any artificial dissipation is obvious in these cases. The MVCB has converged with a rather steep gradient while the averaging scheme fails to converge anymore.

By definition of Reynolds number (based on channel hydraulic diameter), and Fanning friction factor, $f = 2\tau_w/(\rho u_m^2)$, the theoretical value results in, $f = 24/Re$ for laminar regime(Shah and London 1978). Fig.5 shows the variation of f. Re product versus x/Re (ratio of non-dimensional distance from flow entrance to Reynolds number)

for some Re of laminar regime obtained by MVCB scheme. Based on observations, all the curves reached to theoretical value. Also, it was reported that entrance length of channel is about $l_e/Re = 0.011$(Shah and London 1978). As it is shown, numerical solution and reported values are in agreement.
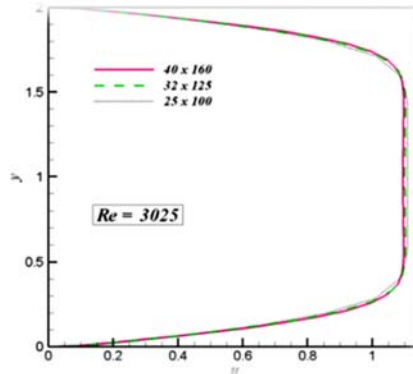

Fig. 3. Comparison of u-velocity profiles at the fully developed region, turbulent channel flow, grid sizes, 25×100, 32×128, and 40×160, clustered grids, *Re*=3025.

In the backward-facing step for laminar regime, the results are compared for *Re = 73* and *Re = 229*(based on step height), with experimental data of Denham and Patrick (1974), and numerical results of Zamzamian and Razavi (2008). Figs. 6 and 7 compares the u-velocity profiles at various distances from the step, and Figs. 8 and 9 the streamlines for the same Reynolds numbers, respectively. Shear stresses on upper and lower walls are shown in Fig. 10. Negative shear stresses denote the backflow and it is clear that at fully developed region the same constant values are reached on the walls. The MVCB scheme behaves well in laminar flows.

For turbulent flow, the results are compared with experimental data of Denham *et al*. (1975) and numerical results of Nithiarasu and Liu (2006). Fig.11 shows the u-velocity profiles at various stations from step for *Re*=3025. Fig.12 compares the streamlines of MVCB with the numerical results of Javadi *et al*. (2008) at *Re*=69610. The modified turbulent viscosity, $\hat{v}$, contours at various Reynolds numbers for backward-facing step flow are shown in Fig.13. As expected, the turbulent effects are dominant at the core of flow and they grow with Reynolds number. The shear stress distributions on the upper and lower walls are presented by Fig.14. As it is seen, the impact of expansion becomes more considerable on the upper wall in turbulent regime. The results confirm adequate accuracy of MVCB scheme in turbulent flow simulations.

Fig.15 shows the streamlines for square lid-driven cavity flow at *Re = 100, and 1000* (based on moving wall velocity and cavity length), obtained with MVCB scheme and compares them with results of Razavi *et al*. (2008). The MVCB scheme was able to reveal flow details in this case. Also,
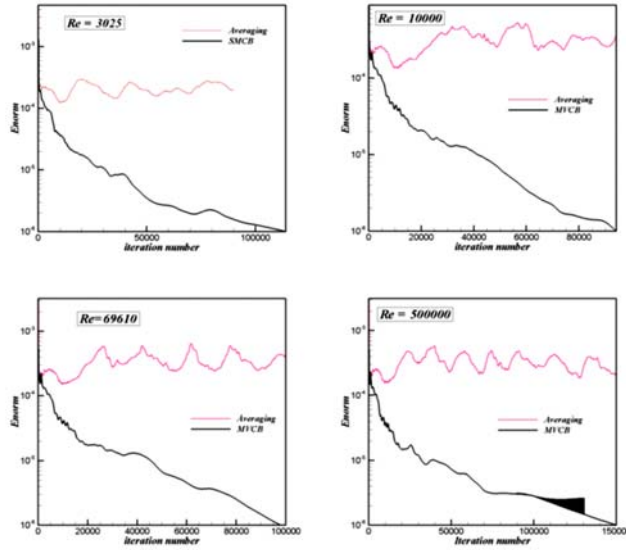
Fig. 4. Comparison of convergence histories for MVCB and averaging schemes, turbulent flow over backward-facing step, *Re*=3025, 60×160, clustered grids and Re= 10000, 69610, 500000, 96×150, clustered grids.

Fig.16 shows the v-velocity profile on the centerline of the cavity parallel with x axis and the u-velocity profile on the centerline of the cavity parallel with y axis which obtained by MVCB scheme and are compared to the first-order scheme of Razavi *et al*. (2008) and Ghia *et al*. (1982) benchmark solution.
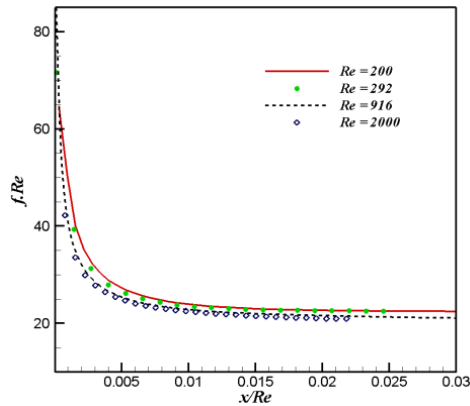
Fig. 5. Variation of f . Re versus x/Re in laminar regime by MVCB scheme for channel flow.

6. CONCLUDING REMARKS

A new scheme (MVCB) for solving laminar and turbulent regimes has been proposed. It is mainly based on the virtual compatibility equations, having conserved multidimensionality. To compute the primitive variables, special combinations of waves are selected such that the spatial derivatives are omitted and straightforward relations are obtained. The distinctive feature of the present method is assuming no directional limitation caused by grid geometry. The majority of past characteristic

models are inevitable in using fluxes normal to cell faces. The proposed formulation could be able to produce all the components of velocity field. Several numerical simulations have been conducted for both the laminar and turbulent regimes in a channel, over backward-facing step, and in square lid-driven cavity at a wide range of Reynolds numbers. For turbulence modeling, the Spalart-Allmaras equation is applied which acted suitably for the selected case studies. The comparison of the results with well-known experimental and numerical data confirms good accuracy and convergence rate for the laminar and turbulence regimes. Another advantage of the MVCB scheme is its capability of capturing flow details at higher Reynolds number without need to any artificial viscosity.
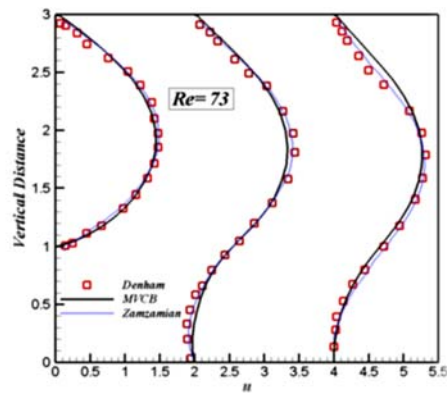

Fig. 6. Comparison of u-velocity of MVCB scheme with numerical results of Zamzamian and Razavi (2008)and experimental data of Denham and Patrick (1974), laminar flow over backward-facing step, *Re*=73.
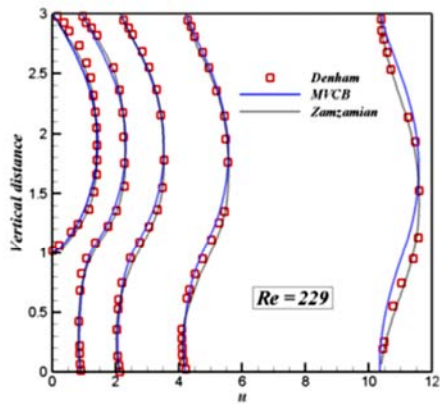
Fig. 7. Comparisons of u-velocity of MVCB scheme with numerical results of Zamzamian and Razavi (2008) and experimental data of Denham and Patrick (1974), laminar flow over backward-facing step, *Re*=229.
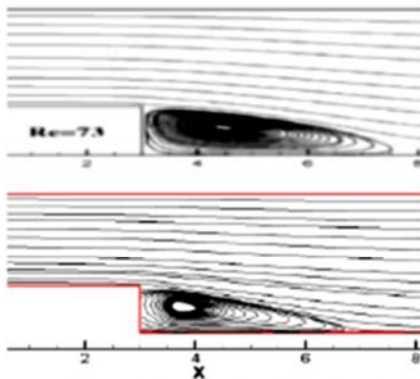

Fig. 8. Comparison of streamlines for MVCB scheme (down) with the results of Zamzamian and Razavi (2008) (up), laminar flow over backward-facing step, *Re*=73.
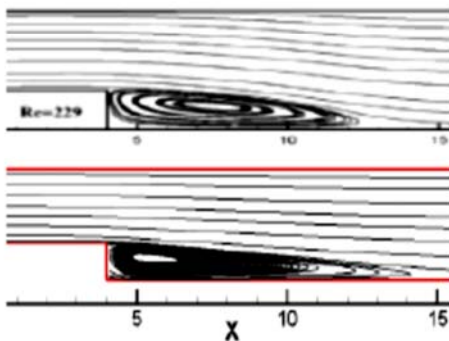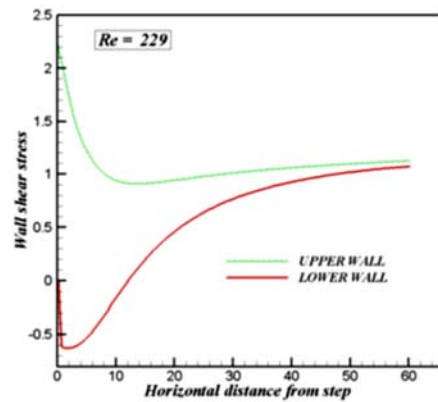

Fig. 9. Comparison of streamlines for MVCB scheme (down) with that of Zamzamian and Razavi (2008)(up) for laminar flow over backward-facing step, *Re*=229.
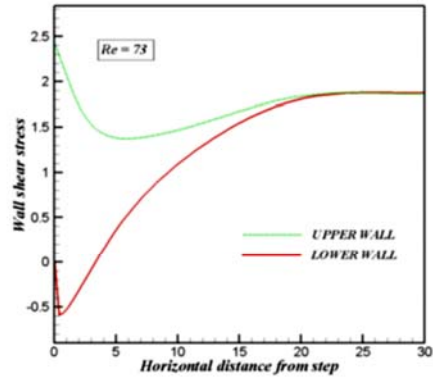

Fig. 10. Shear stresses on the upper and lower walls versus horizontal distance from step, laminar flow over backward-facing step, *Re*=73 and 229, MVCB scheme.
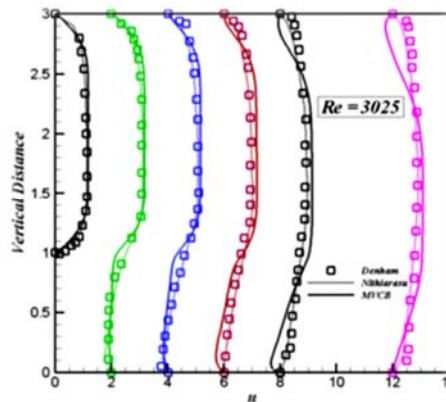

Fig.11 Comparison of u-velocity of MVCB scheme with numerical results of Nithiarasu and Liu (2006) and experimental data of Denham *et al*. (1975), turbulent flow over backward-facing step, *Re*=3025.
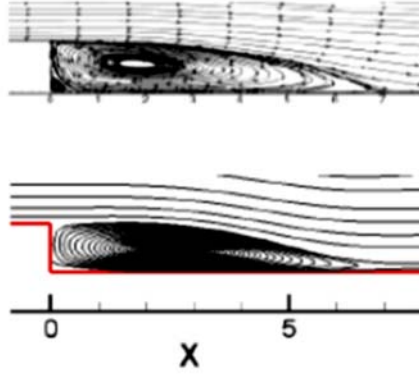
Fig. 12. Comparison of streamlines for MVCB scheme (down) with numerical results of Javadi *et al*. (2008) (up) for turbulent flow over backward-facing step, *Re*=69610.
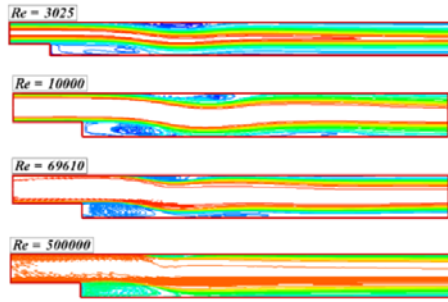

Fig. 13. Modified turbulent viscosity ($\hat{v}$), flow over backward-facing step, *Re*=3025, 10000, 69610, and 500000, MVCB scheme.

APPENDIX A

Fig.17 shows a quadrilateral cell (i , j) and its faces. As mentioned, Eq. (5) is discretized form of Eq. (1). The right hand side of Eq. (5) is shown upon to subscript *k* as follow,

$$Q_{ij1} = \beta^2 \left[\sum_{l=1}^{4} (u\Delta y - v\Delta x)_l \right]_{ij} \tag{A-1}$$

$$\begin{aligned}
Q_{ij2} &= -\alpha \left[u \sum_{l=1}^{4} (u\Delta y - v\Delta x)_l \right]_{ij} \\
&+ \sum_{l=1}^{4} \left\{ \left[P + u^2 - \left(\frac{1+v_T}{Re}\right)\frac{\partial u}{\partial x} \right]_l \Delta y_l \right. \\
&\left. - \left[uv - \left(\frac{1+v_T}{Re}\right)\frac{\partial u}{\partial y} \right]_l \Delta x_l \right\}_{ij}
\end{aligned} \tag{A-2}$$

$$\begin{aligned}
Q_{ij3} &= -\alpha \left[v \sum_{l=1}^{4} (u\Delta y - v\Delta x)_l \right]_{i,j} \\
&+ \sum_{l=1}^{4} \left\{ \left[uv - \left(\frac{1+v_T}{Re}\right)\frac{\partial v}{\partial x} \right]_l \Delta y_l \right. \\
&\left. - \left[P + v^2 - \left(\frac{1+v_T}{Re}\right)\frac{\partial v}{\partial y} \right]_l \Delta x_l \right\}_{ij}
\end{aligned} \tag{A-3}$$

$$\begin{aligned}
Q_{ij4} &= -\alpha \left[\hat{v} \sum_{l=1}^{4} (u\Delta y - v\Delta x)_l \right]_{ij} \\
&+ \sum_{l=1}^{4} \left\{ \left[u\hat{v} - \left(\frac{1+c_{b2}}{Re\sigma}\right)(1 + \hat{v})\frac{\partial \hat{v}}{\partial x} \right]_l \Delta y_l \right. \\
&\left. - \left[v\hat{v} - \left(\frac{1+c_{b2}}{Re\sigma}\right)(1 + \hat{v})\frac{\partial \hat{v}}{\partial y} \right]_l \Delta x_l \right\}_{ij} \\
&- A_{ij} \left\{ c_{b1}(1 - f_{t2})\hat{s}\hat{v} \right. \\
&- \frac{c_{b2}}{Re\sigma}(1 + \hat{v})\left(\frac{\partial^2 \hat{v}}{\partial x^2} + \frac{\partial^2 \hat{v}}{\partial y^2}\right) \\
&\left. - \frac{1}{Re}\left[c_{w1}f_w - \frac{c_{b1}}{\kappa^2}f_{t2} \right]\left(\frac{\hat{v}}{y}\right)^2 \right\}_{ij}
\end{aligned} \tag{A-4}$$

where, 1,2,3, and 4 indices which are replaced for *k* subscript, indicate the rows of matrices in Eq. (1), i.e., continuity, x-momentum, y-momentum, and turbulent model equations, respectively. Summations are computed for quantities on faces, in counter-clockwise direction.

APPENDIX B

Eq. (11), for θ = 0, $\frac{\pi}{2}$, π, and $\frac{3\pi}{2}$ results in,

$$\begin{aligned}
\eta(0) + u &= \frac{\beta^2}{\eta(0)} \\
\eta(\pi) - u &= \frac{\beta^2}{\eta(\pi)} \\
\eta(\pi/2) + v &= \frac{\beta^2}{\eta(\pi/2)} \\
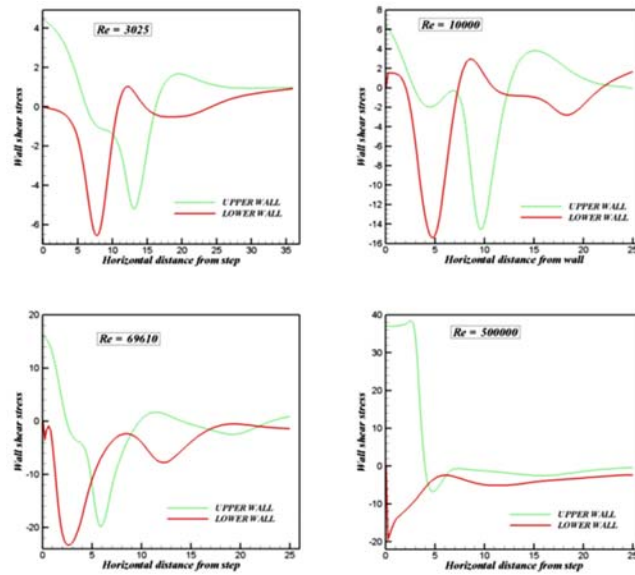\eta(3\pi/2) - v &= \frac{\beta^2}{\eta(3\pi/2)}
\end{aligned} \tag{B-1}$$

Fig. 14. Shear stresses on the upper and lower walls versus horizontal distance from step, turbulent flow over backward-facing step, *Re*=3025, 10000, 69610 and 500000, MVCB scheme.
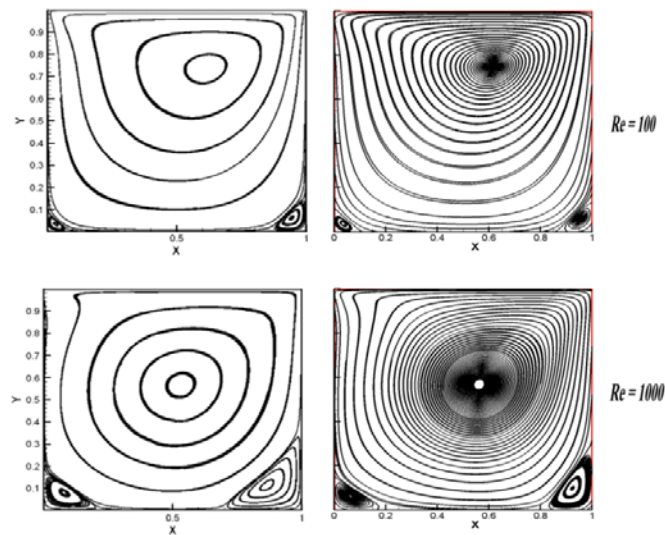

Fig. 15. Streamlines for lid driven cavity at Re = 100 (up) and Re = 1000, results of Razavi *et al*. (2008) (left), MVCB (right).
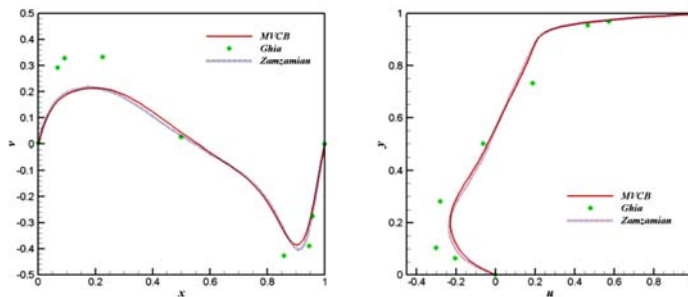

Fig. 16. The v-velocity profile on centerline of cavity parallel with x axis (left), and u-velocity profile on centerline of cavity parallel with y axis (right), for Re = 1000 by MVCB scheme compared with the first order scheme of Razavi *et al*. (2008) and benchmark solution of Ghia *et al*. (1982).
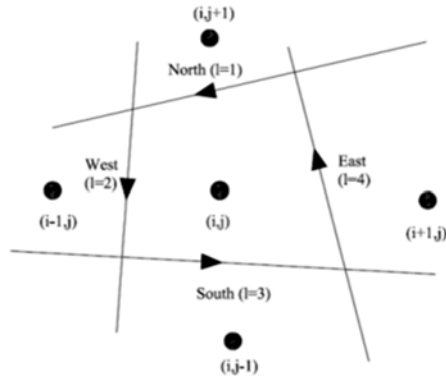
Fig. 17. Stencil of a quadrilateral cell.

The following expressions can be obtained by applying Eqs. (B-1) for Eq. (17),

$$-\eta(0)D^0 u + D^0 P + \beta^2 \frac{\partial v}{\partial y} - v \frac{\partial P}{\partial y} = 0 \qquad \text{(B-2)}$$

$$\eta(\pi)D^\pi u + D^\pi P + \beta^2 \frac{\partial v}{\partial y} - v \frac{\partial P}{\partial y} = 0 \qquad \text{(B-3)}$$

$$-\eta(\pi/2)D^{\pi/2} v + D^{\pi/2} P + \beta^2 \frac{\partial u}{\partial x} - u \frac{\partial P}{\partial x} = 0 \qquad \text{(B-4)}$$

$$\eta(3\pi/2)D^{3\pi/2} v + D^{3\pi/2} P + \beta^2 \frac{\partial u}{\partial x} - u \frac{\partial P}{\partial x} = 0 \qquad \text{(B-5)}$$

Eq. (19) results from subtraction of Eq. (B-3) from Eq. (B-2). Similarly, Eq. (20) is obtained from Eqs. (B-5) and (B-4).

The non-dimensional continuity equation results in,

$$\beta^2 \left(\frac{\partial u}{\partial x} + \frac{\partial v}{\partial y} \right) = -\frac{\partial P}{\partial t} \qquad \text{(B-6)}$$

According to Eq. (B-6) and definition of D^s, i.e. Eq. (15), summation of Eqs. (B-2) to (B-5) results in Eq. (21).

REFERENCES

Blazek, J. (2001). *Computational fluid dynamics*: Principle and applications, 1st/Ed. Elsevier.

Boukir, K., Y. Maday and B. Métivet (1994). A high order characteristics method for the incompressible Navier—Stokes equations. *Computer Methods in Applied Mechanics and Engineering 116, 211-218.*

Calhoon, W. and R. Roach (1997). A naturally upwinded conservative procedure for the incompressible Navier-Stokes equations on non-staggered grids. *Computers and Fluids 26, 525-545.*

Chorin, A. J. (1997). A Numerical Method for Solving Incompressible Viscous Flow Problems. *Journal of Computational Physics 135, 118-125.*

Denham, M., P. Briard and M. Patrick (1975). A directionally-sensitive laser anemometer for velocity measurements in highly turbulent flows. *Journal of Physics E: Scientific Instruments 8, 681.*

Denham, M. and M. Patrick (1974). Laminar flow over a downstream-facing step in a two-dimensional flow channel. *Trans. Inst. Chem. Engrs 52, 361-367.*

Drikakis, D., P. Govatsos and D. Papantonis (1994). A characteristic‑based method for incompressible flows. *International Journal for Numerical Methods in Fluids 19, 667-685.*

Ghia, U., K. N. Ghia and C. T. Shin (1982). High-Re solutions for incompressible flow using the Navier-Stokes equations and a multigrid method. *Journal of Computational Physics 48, 387-411.*

Govatsos, P. and D. Papantonis (2000). A characteristic based method for the calculation of three‑dimensional incompressible, turbulent and steady flows in hydraulic turbomachines and installations. *International Journal for Numerical Methods in Fluids 34, 1-30.*

Guermond, J. L., P. Minev and J. Shen (2006). An overview of projection methods for incompressible flows. C*omputer Methods in Applied Mechanics and Engineering 195, 6011-6045.*

Harichandan, A. B., and A. Roy (2012). CFR: A Finite Volume Approach for Computing Incompressible Viscous Flow. *Journal of Applied Fluid Mechanics 5, 39-52.*

Hirsch, C. (1988). *Numerical Computation of Internal and External Flows: Fundamentals of Numerical Discretization, Wiley, New York.*

Javadi, K., M. Darbandi and M. Taeibi-Rahni (2008). Three-dimensional compressible–incompressible turbulent flow simulation using a pressure-based algorithm. *Computers & Fluids 37, 747-766.*

Neofytou, P. (2007). Revision of the characteristics-based scheme for incompressible flows. *Journal of Computational Physics 222, 475-484.*

Nithiarasu, P. and C. B. Liu (2006). An artificial compressibility based characteristic based split (CBS) scheme for steady and unsteady turbulent incompressible flows. *Computer Methods in Applied Mechanics and Engineering 195, 2961-2982.*

Pappou, T. and S. Tsangaris (1997). Development of an artificial compressibility methodology using flux vector splitting. International *Journal for Numerical Methods in Fluids 25, 523-545.*

Razavi, S., K. Zamzamian and A. Farzadi (2008). Genuinely multidimensional characteristic‑based scheme for incompressible flows. *International Journal for Numerical Methods in Fuids 57, 929-949.*

Rogers, S. E. and D. Kwak (1991). An upwind

differencing scheme for the incompressible Navier–Strokes equations. *Applied Numerical Mathematics 8, 43-64.*

Shah, R. K. and A. L. London (1978). Chapter VI - *Parallel Plates. In Laminar Flow Forced Convection in Ducts* (R. K. S. L. London, ed.), 153-195. Academic Press.

Su, X., Y. Zhao and X. Huang (2007). On the characteristics-based ACM for incompressible flows. *Journal of Computational Physics 227, 1-11.*

Zamzamian, K., and Razavi, S. E. (2008). Multidimensional upwinding for incompressible flows based on characteristics. Journal of *Computational Physics 227, 8699-8713.*

Zhao, Y., and Zhang, B. (2000). A high-order characteristics upwind FV method for incompressible flow and heat transfer simulation on unstructured grids. *Computer Methods in Applied Mechanics and Engineering 190, 733-756.*

Zienkiewicz, O., Morgan, K., Sai, B., Codina, R., and Vasquez, M. (1995). A general algorithm for compressible and incompressible flow— Part II. Tests on the explicit form. International *Journal for Numerical Methods in Fluids 20, 887-913.*

Zienkiewicz, O. C., and Codina, R. (1995). A general algorithm for compressible and incompressible flow—Part I. the split, characteristic‐based scheme. International *Journal for Numerical Methods in Fluids 20, 869-885.*

Zucrow, M. J., and Hoffman, J. D. (1977). *Gas dynamics,Multidimensional flow*, New York, John Wiley and Sons, Inc.